Electronic Supplementary Information

Gas-liquid-liquid three-phase flow pattern and pressure drop in a microfluidic chip: similarities with gas-liquid/liquid-liquid flows

Jun Yue,[a] Evgeny V. Rebrov[b] and Jaap C. Schouten*[a]

[a] *Laboratory of Chemical Reactor Engineering, Department of Chemical Engineering and Chemistry, Eindhoven University of Technology, P.O. Box 513, 5600 MB Eindhoven, The Netherlands*

[b] *School of Chemistry and Chemical Engineering, Queen's University Belfast, Belfast BT9 5AG, United Kingdom*

* Corresponding author

Jaap C. Schouten (j.c.schouten@tue.nl)

Table of contents

Part I. Supplementary movies S1-S7

In this part, captions for the supplementary movies are given with an image shown for each movie. The quality of these pictures has been adjusted for a better view.

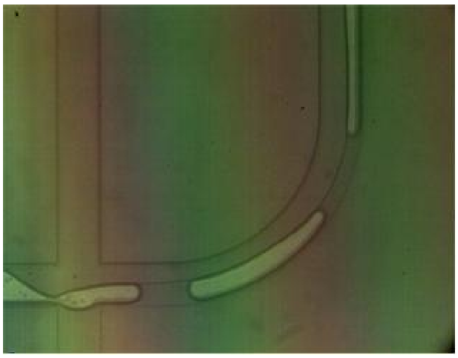

Movie S1 Flow configuration at the cross-flow mixer under the operating conditions relevant to the formation of the three-phase slug flow pattern. $j_{G,\ STP}$ = 30.4 mm/s, j_D = 10.1 mm/s, j_W = 40.5 mm/s. The flow configuration here is the same as that observed in the parallel-slug flow pattern, that is, a side-by-side flow between water and decane with nitrogen bubbles being encapsulated in the decane phase. At a downstream location, viz. at a distance of 5 mm from the cross-flow mixer, the breakup of the formed parallel flow occurs, thus generating a three-phase slug flow, as further shown in Movie S2.

Movie S2 Three-phase slug flow pattern generation at a distance of 5 mm from the cross-flow mixer. $j_{G,\ STP}$ = 30.4 mm/s, j_D = 10.1 mm/s, j_W = 40.5 mm/s. The advancing decane tip can be seen and a 'nitrogen-in-decane' droplet is generated by the breakup of the decane-water parallel flow previously formed in the cross-flow mixer.

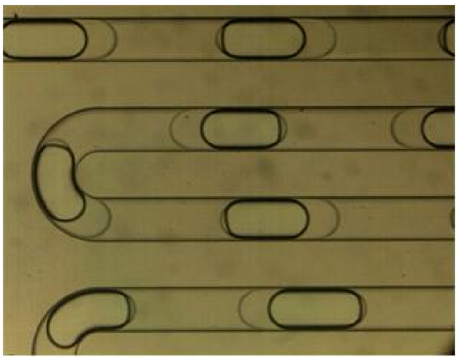

Movie S3 Three-phase slug flow pattern in the left part of microchannel segments 1-2. $j_{G,\ STP}$ = 30.4

mm/s, j_D = 10.1 mm/s, j_W = 40.5 mm/s. A single elongated nitrogen bubble is seen to be encapsulated in a decane droplet. Thus formed 'nitrogen-in-decane' droplet travels intermittently with the water slug along the microchannel.

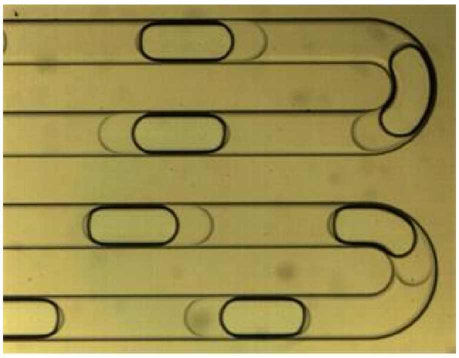

Movie S4 Three-phase slug flow pattern in the right part of microchannel segments 4-5. $j_{G,\ STP}$ = 30.4 mm/s, j_D = 10.1 mm/s, j_W = 40.5 mm/s.

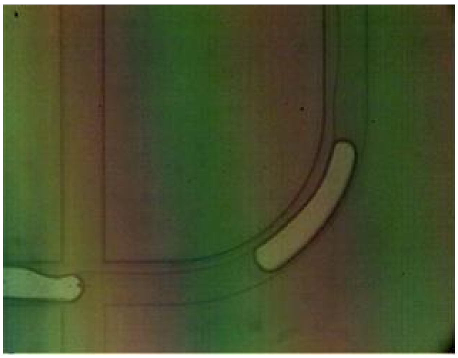

Movie S5 Parallel-slug flow pattern after the cross-flow mixer. $j_{G,\ STP}$ = 30.4 mm/s, j_D = 40.5 mm/s, j_W = 10.1 mm/s. A side-by-side parallel flow between decane and water is formed while the elongated nitrogen bubbles are generated in the decane phase forming a local slug flow.

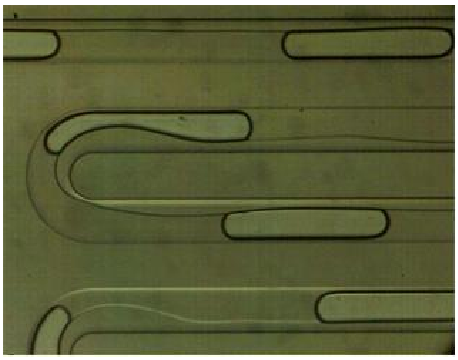

Movie S6 Parallel-slug flow pattern in the left part of microchannel segments 1-2. $j_{G,\ STP}$ = 30.4 mm/s, j_D = 40.5 mm/s, j_W = 10.1 mm/s. The interface between the decane slugs and the water phase is always observed at the same transverse position in the straight part of the microchannel. However, the width of the water stream changes to some extent in the curved sections of the microchannel.

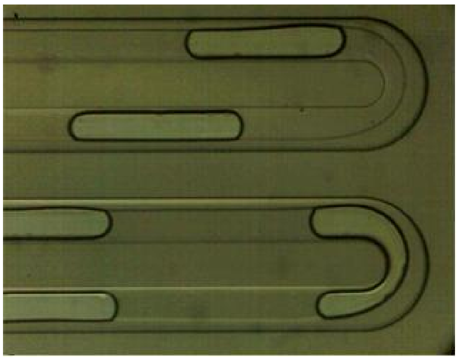

Movie S7 Parallel-slug flow pattern in the right part of microchannel segments 4-5. $j_{G,\,STP}$ = 30.4 mm/s, j_D = 40.5 mm/s, j_W = 10.1 mm/s. A planar liquid-liquid interface is assumed in this flow pattern especial for the region where the decane slugs meet the adjacent water stream. In the region containing bubbles, a temporarily curved decane-water interface is observed as the bubbles expand towards the water side.

Part II. Supplementary notes S1-S4

Note S1 Determination of the laminar friction constant in the present microchannel geometry

The microchannel has a cross section close to a rectangle with rounded bottom (as shown in Fig. 1a of the paper). The top width (W) is 300 μm and the height (H) 60 μm. The shape of the two side walls is a 1/4 circular arc with a radius of H. This gives a hydraulic diameter (d_h) of the present microchannel to be 98 μm derived from

$$d_h = \frac{4(W-2H)H + 2\pi H^2}{2W - 2H + \pi H} \tag{S1}$$

The correlation for the laminar friction constant ($C = f\,Re$; f is the laminar friction factor and Re the Reynolds number) in this microchannel geometry is not available in the literature. Therefore, an axisymmetric 3D simulation of water flow in this microchannel was performed to obtain the exact solution to the laminar friction factor using Comsol Multiphysics (Version 4.3, Comsol AB, USA). The flow is assumed to be incompressible and steady. The computational domain consists of half of a straight microchannel section with a length of 2 mm (Fig. S1a). The governing mass and momentum conservation equations are given by

$$\rho \nabla \cdot u = 0 \tag{S2}$$

$$\rho(u \cdot \nabla)u = -\nabla P + \mu \nabla \cdot \left(\nabla u + (\nabla u)^T\right) + \rho g \tag{S3}$$

where P is the pressure and g is the gravitational acceleration. ρ, μ, and u denote the density, viscosity, and velocity vector of the fluid. Eqn (S2) and (S3) were implemented on the computational domain using the 'Lamina Flow' interface in Comsol. No slip boundary condition (u = 0) was applied at the walls of the microchannel and a symmetric boundary condition (no penetration and vanishing shear stresses) was used for the axis plane of symmetry. A uniform velocity was imposed at the inlet and a zero pressure constraint was set at the outlet. The 3D computational domain was meshed with triangular prisms, that is, by sweeping the mesh from the microchannel cross-sectional face at inlet along the domain (increasing y direction) to the opposite cross-sectional face at outlet. An exponentially decreasing distribution of mesh elements along the domain was used. Then the segregated solver was used to solve the governing equations.

The exact solution to eqn (S2) and (S3) was obtained under an inlet average velocity (U_{avg}) of water at 10 mm/s and a temperature of 20 ºC corresponding to $Re \approx 1$ ($Re = d_h U_{\mathrm{avg}} \rho / \mu$). With the obtained pressure field, the average pressure at various axis positions (y direction) was calculated by performing a surface integration over the microchannel cross section. To eliminate the influence of entrance and exit effects, the simulated pressure drop (ΔP_{num}) was only considered in the middle part of the simulated microchannel section the length of which (L_1) is 1 mm (i.e., at a distance of 0.5 mm from the inlet and outlet). Then, the laminar friction constant was derived as

$$C = \frac{2\Delta P_{\mathrm{num}} d_h^2}{\mu L_1 U_{\mathrm{avg}}} \tag{S4}$$

Fig. S1b shows the mesh dependence of thus obtained C value. C approaches a converged value of about 75.33 as the mesh number reaches above 200,000 (minimum element size at 0.3 μm; maximum element size at 1.6 μm over the cross section; element number along y direction at 30) after which an increase of the mesh number only leads to a marginal increase in C.

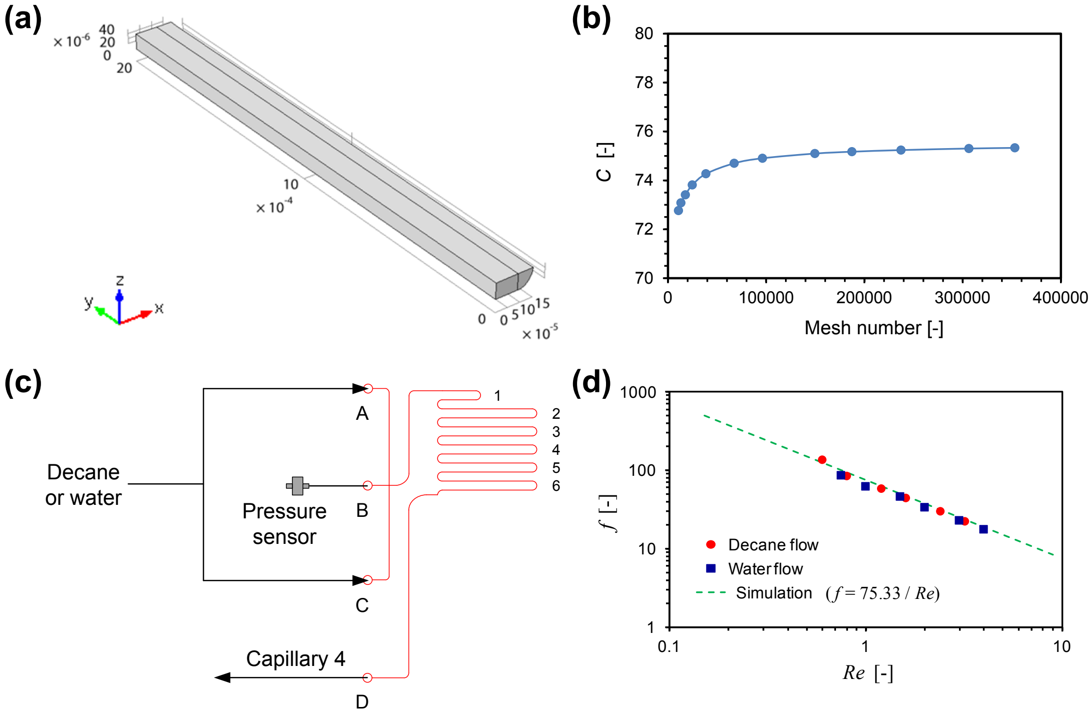

Fig. S1 (a) Computational domain in Comsol simulation. The dimensions are in m. (b) C as a function of the number of mesh elements. The mesh number was increased by decreasing the maximum and minimum sizes of mesh elements over the microchannel cross section. (c) Schematic view of the fluidic connection with the chip and pressure measuring method in single-phase flow experiments. (d) The experimentally determined f as a function of Re and its comparison with the prediction given by the simulation.

The correctness of this converged value is further corroborated by our experimental measurements with single-phase flows of either water or decane in the microfluidic chip. Fig. S1c shows the fluidic connection with the chip and the pressure measuring method. The decane (or water) flow was divided into two substreams that were subsequently introduced into the chip via ports A and C. The fluid then passed the cross-flow mixer and further travelled in the chip along segments 1-6 before being guided out of the chip via port D. The rest part of the chip was therefore unused and was filled with the stagnant fluid. The pressure at the cross-flow mixer was measured by a pressure sensor connected to port B. Experiments were performed at a fluid flow rate up to 40 μl/min. Similar to the three-phase and two-phase flow studies in the chip, the pressure drop during fluid laminar flow over the active microchannel length (L) of 14 cm was measured as the pressure difference in the experiments with the chip and the reference experiments in which the chip was replaced by an external PEEK cross-flow mixer (1.25 mm in diameter, each fluid branch about 4 mm long) under identical flow rate conditions. Then, the laminar friction factor (f) was measured as

$$f = \frac{2\Delta P_{\mathrm{exp}} d_h}{\rho L U_{\mathrm{avg}}^2} \tag{S5}$$

where ΔP_{exp} is the experimentally determined laminar pressure drop. Eqn (S5) is derived based on the consideration that the curvature-induced secondary flow in the curved parts of the microchannel (if present) did not contribute appreciably to the total frictional pressure drop. This is a reasonable assumption given very small Re involved (< 10) and very low fraction of the curved parts as compared to the straight parts of the microchannel.[1] Fig. S1d depicts thus obtained f value as a function of Re for both water and decane single-phase flow experiments. The prediction according to the Comsol simulation is also shown. The experimental data are shown consistent with the predictions.

It should be mentioned that the obtained C value of 75.33 is close to that of 76.30 for a rectangular microchannel with the same height (H = 60 μm) and width (W = 300 μm). The latter value is calculated using the existing correlation in the literature given by eqn (S6).[2] This match is reasonable since the shape of the current microchannel is close to an ideal rectangle.

$$C = 96\left(1 - 1.3553\alpha + 1.9467\alpha^2 - 1.7012\alpha^3 + 0.9564\alpha^4 - 0.2537\alpha^5\right) \quad \text{(S6)}$$

where α is the aspect ratio defined as $\alpha = H / W$ at $H \leq W$ and otherwise $\alpha = W / H$.

Note S2 Dependence of length parameters (L_S, L_B, L_{drop}) on the flow ratio during the two-phase and three-phase flow studies in the chip

For the calculation of the total frictional pressure drop during two-phase and three-phase slug flows in the microchannel on the chip, the length of liquid slugs (L_S) and that of droplets or bubbles ($L_D = L_B$ or L_{drop}) need to be known, as specified in eqn (6) of the paper. When it comes to pressure drop estimation in the parallel-slug flow pattern using eqn (12) of the paper, the length of the nitrogen bubble and that of the decane slug which forms a side-by-side flow with respect to water are needed as input. For each flow pattern described here, the corresponding length parameters were obtained from multiple images captured in the middle part of microchannel segments 3-5. The definition of these parameters has been illustrated in the insets of Fig. 5, Fig. 7, and in Fig. 8a of the paper for the two-phase slug flow, three-phase slug flow, and parallel-slug flow patterns, respectively.

The dependence of the measured length parameters on the operating conditions for each flow pattern is presented in Figs. S2a-S2d. For the nitrogen-decane and nitrogen-water slug flow patterns, as the nitrogen to liquid flow ratio (j_G / j_L) increases, the bubble length increases and the liquid slug length tends to decrease in general (Fig. S2a). Similar trend was observed for the decane-water slug flow pattern (Fig. S2b). The length of decane droplets increases and that of the water slug decreases upon increasing the decane to water flow ratio (j_D / j_W). In the latter case the droplet size remains the same throughout the entire length of the microchannel due to incompressibility of liquids. This is in contrast to the former case in which a bubble, after being produced in the cross-flow mixer, tends to expand along the microchannel as a result of decreasing absolute pressure towards the outlet of the microchannel. As shown in Fig. S2c for the three-phase slug flow pattern, the length of a 'nitrogen-in-decane' droplet (L_{drop}) shows an increase upon increasing the nitrogen to decane flow ratio (j_G / j_D). This is consistent with the fact that this flow pattern is realized first by the formation of nitrogen bubbles in the decane phase which travels alongside with water for some length, and then by the formation of composite droplets due to the breakup of the decane-water parallel flow further downstream (see Fig. 2a of the paper). Therefore, the droplet size in this case is directly related to the flow ratio between nitrogen and decane. The water slug length (L_S) in this case also seems to increase with the increasing nitrogen to decane flow ratio.

In the case of the parallel-slug flow pattern (Fig. S2d), the size of the nitrogen bubble and the decane slug as a function of j_G / j_D exhibits similar dependence to the case of the nitrogen-decane slug flow pattern as shown in Fig. S2a. This behavior is expected as the nitrogen bubbles are produced in the decane phase and the parallel flow of water does not disturb the local nitrogen-decane slug flow.

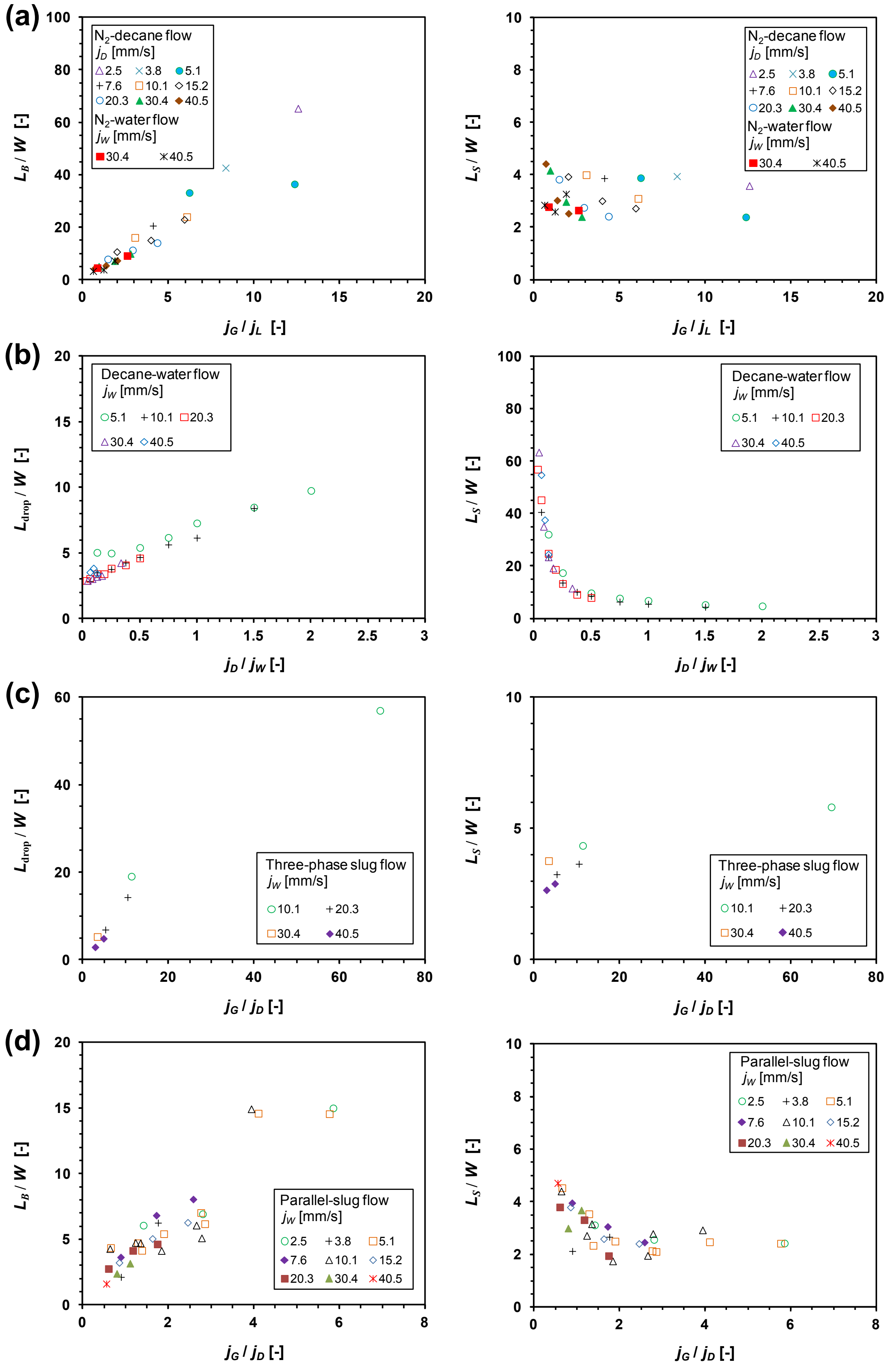

Fig. S2 (a) Length of nitrogen bubbles (left) and liquid slugs (right) as a function of the nitrogen to liquid flow ratio in the gas-liquid slug flow pattern. j_L is the superficial liquid velocity (= j_W for the nitrogen-water slug flow; = j_D for the nitrogen-decane slug flow). (b) Length of decane droplets (left) and water slugs (right) as a function of the decane to water flow ratio in the liquid-liquid slug flow pattern. (c) Length of 'nitrogen-in-decane' droplets (left) and water slugs (right) as a function of the nitrogen to decane flow ratio in the three-phase slug flow pattern. (d) Length of nitrogen bubbles (left) and decane slugs (right) as a function of the nitrogen to decane flow ratio in the parallel-slug flow pattern. All length parameters were obtained from image analysis at the middle part of microchannel segments 3-5 on the chip. In (a), (c) and (d), j_G is the average superficial gas velocity evaluated using the nitrogen density based on the average pressure in the microchannel.

The physical mechanisms governing the bubble and droplet formation process at or near the cross-mixer have to be well examined to derive functional dependencies between the length parameters (L_S, L_B, L_{drop}) and the corresponding flow ratios for each flow pattern. The effect of gas compressibility needs to be considered in order to predict the axial variation of the bubble length along the microchannel. A detailed study on this topic is beyond the scope of this paper.

Note S3 Determination of the relation between Q^* and β from Comsol simulation

For the flow of one identical fluid through the present microchannel that is divided into two regions by a separation line at $x = W/2 - W_1$ (see Fig. S3a), the volumetric flow rate in the region to the right of the separation line (Q_{right}) and the total flow rate over the cross section (Q_{tot}) are calculated by integration of the velocity field (v) over the right section of the microchannel and the entire microchannel cross section, respectively. That is,

$$Q_{\mathrm{right}} = \int_{W/2-W_1}^{W/2} \left(\int_0^H v dz \right) dx \tag{S7}$$

$$Q_{\mathrm{tot}} = 2\int_0^{W/2} \left[\int_0^H v dz \right] dx \tag{S8}$$

The velocity field in the microchannel for fully developed laminar flow of water is shown in Fig. S3b. This field was obtained with Comsol as described in Note S1. The computational domain represents half of the microchannel geometry due to symmetry of the microchannel cross section (see Fig. S1a).

Since we found out that the decane-water parallel flow in the present microchannel could be effectively treated as a single-phase laminar flow of water, it is reasonable to assume that for a given interfacial position ($\beta = W_1 / W$) in such parallel flow case, the flow ratio of water to the decane-water mixture ($Q^* = Q_W / (Q_W + Q_D) = j_W / (j_W + j_D)$) can be estimated from

$$Q^* = \frac{Q_{\mathrm{right}}}{Q_{\mathrm{tot}}} = \frac{\int_{W/2-W_1}^{W/2} \left(\int_0^H v dz \right) dx}{2\int_0^{W/2} \left[\int_0^H v dz \right] dx} \tag{S9}$$

Thus determined Q^* as a function of β is shown in Fig. 8b of the paper, which can indeed well describe the experimentally measured relation between β and Q^* in the decane-water parallel flow pattern observed in the microchannel.

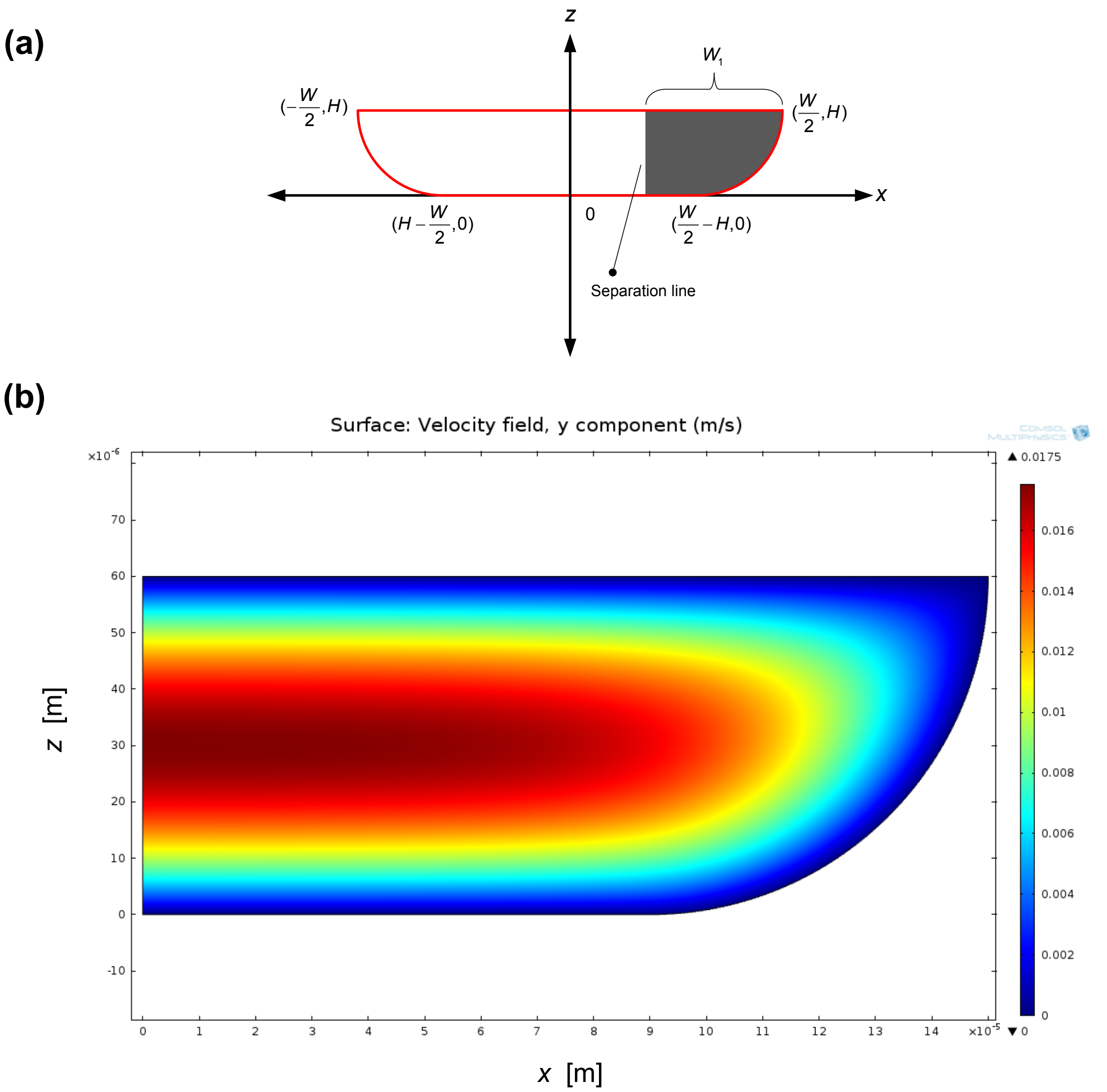

Fig. S3 (a) Schematic view showing the microchannel cross section (W = 300 μm, H = 60 μm) on an x-z coordinate system. The coordinates of four vertices defining the top width and the bottom width are shown. The cross section is divided into two regions by a separation line at $x = W/2 - W_1$. The region to the right of the separation line is shadowed. (b) The simulated y-component velocity field (v) of water in half of the microchannel cross section at y = 0.5 mm. Here y is the axial direction as shown in Fig. S1a. At this axial distance, the flow is already fully developed and the x- and z-components of the velocity field are zero. The simulation was carried out under an inlet average velocity of water of 10 mm/s and a temperature of 20 ºC. Further simulation details are given in Note S1.

Note S4 Estimation of the effective hydraulic diameter for nitrogen bubbles moving in the decane phase under parallel-slug flow

In the parallel-slug flow pattern, the nitrogen bubbles are present in the decane phase which flows parallel to water. Under the assumption that the decane film around the bubble body can be neglected, the pressure drop across the bubble body (ΔP_{body}) is calculated as

$$\Delta P_{\mathrm{body}} = \frac{nC\mu_{\mathrm{G}} L_{\mathrm{body}} U_B}{2d_e^2} \tag{S10}$$

Here d_e is the effective hydraulic diameter associated with the local nitrogen-decane slug flow through the microchannel cross-sectional area which is not occupied by water (i.e., the colored area as shown in Figs. S4a and S4b). An estimation of d_e is made according to the definition of the hydraulic diameter as $d_e = 4A_e / S_e$, where A_e is the cross-sectional area for the local nitrogen-decane slug flow and S_e the wetted perimeter thereof. The shear stresses at the wall and at the interface are expected to be comparable if the bubble body flows through the entire part of this colored area. In this case, both the microchannel wall and the decane-water interface should be taken into account for the wetted perimeter.[3] This also implicates that in real situations where a decane film surrounds the bubble body, the friction exerted on the bubble body by the film in contact with the microchannel wall is comparable to the friction by the film at the interface. Thereby the bubble body flows as if it was in a microchannel all walls of which were covered by the surrounding film and ΔP_{body} can be approximated with eqn (S10) by ignoring the film presence.

Then, it is easy to show that at $H \leq W_1 \leq W/2$ (cf. Fig. S4a),

$$A_e = \frac{\pi}{4}H^2 + \left(W - W_1 - H\right)H \tag{S11}$$

$$S_e = \left(W - W_1\right) + \frac{\pi}{2}H + \left(W - 2H - \left(W_1 - H\right)\right) + H = 2W - 2W_1 + \frac{\pi}{2}H \tag{S12}$$

And at $W_1 < H$ (cf. Fig. S4b),

$$A_e = \frac{\pi}{4}H^2 + \left(W - 2H\right)H + \frac{H - W_1}{2}\sqrt{2HW_1 - W_1^2} + \frac{H^2}{2}\arcsin\left(\frac{H - W_1}{H}\right) \tag{S13}$$

$$\begin{aligned} S_e &= \left(W - W_1\right) + \frac{\pi}{2}H + \left(W - 2H + H\arcsin\left(\frac{H - W_1}{H}\right)\right) + \sqrt{2HW_1 - W_1^2} \\ &= 2W - W_1 + \left(\frac{\pi}{2} - 2 + \arcsin\left(\frac{H - W_1}{H}\right)\right)H + \sqrt{2HW_1 - W_1^2} \end{aligned} \tag{S14}$$

d_e is thus represented by

$$d_e = \frac{\pi H^2 + 4\left(W - W_1 - H\right)H}{2W - 2W_1 + \frac{\pi}{2}H} \tag{S15}$$

at $H \leq W_1 \leq W/2$ and by

$$d_e = \frac{\pi H^2 + 4\left(W - 2H\right)H + 2\left(H - W_1\right)\sqrt{2HW_1 - W_1^2} + 2H^2\arcsin\left(\frac{H - W_1}{H}\right)}{2W - W_1 + \left(\frac{\pi}{2} - 2 + \arcsin\left(\frac{H - W_1}{H}\right)\right)H + \sqrt{2HW_1 - W_1^2}} \tag{S16}$$

at $W_1 < H$. Thus estimated values of d_e are found to range from 83.4 to 98.9 μm as β (= W_1 / W) is varied between 0 and 0.5 (cf. Fig. S4c). Thus, d_e is very close to the hydraulic diameter of the present microchannel (d_h = 98 μm as calculated with eqn (S1) shown in Note S1), the maximum deviation between them being about 15% at $\beta = 0.5$.

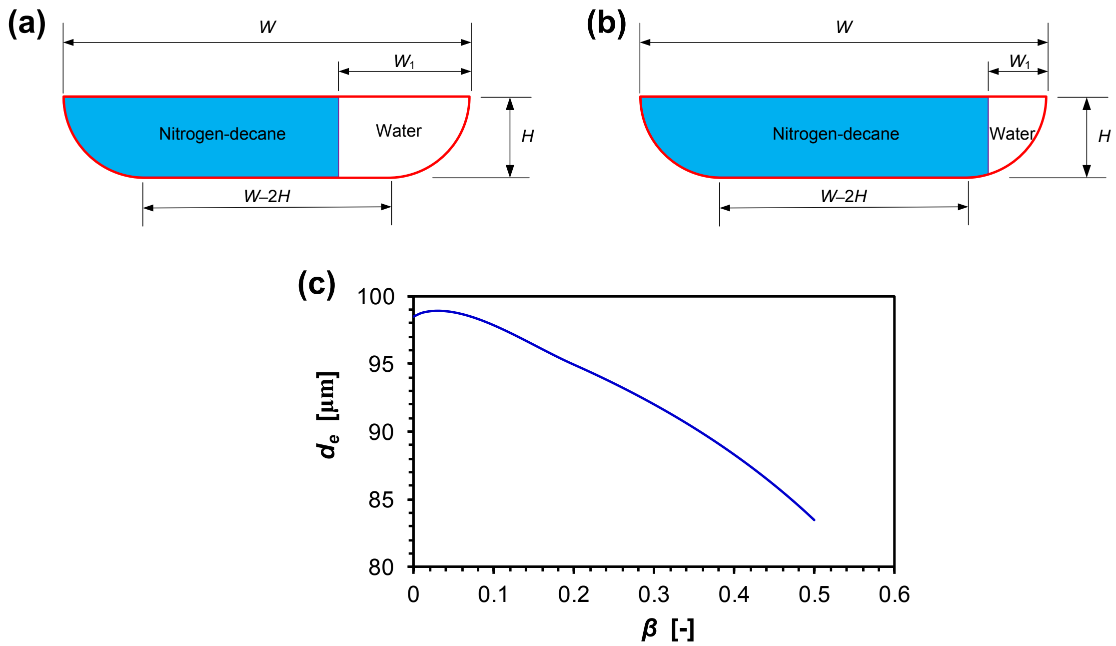

Fig. S4 Schematic diagrams showing the current microchannel cross section (W = 300 µm, H = 60 µm) separated into two regions under parallel-slug flow at (a) $H \leq W_1 \leq W/2$ and (b) $W_1 < H$. (c) The dependence of d_e determined from eqn (S15) and (S16) on β. In (a) and (b), water occupies the uncoloured region which has a width of W_1 as viewed from the microchannel top. The region for the local nitrogen-decane slug flow is colored in light blue.

Supplementary references

1 A. A. Donaldson, D. M. Kirpalani and A. Macchi, *Chem. Eng. Process.*, 2011, **50**, 877-884.

2 R. K. Shah and A. L. London, *Laminar Flow Forced Convection in Ducts*, Academic Press, New York, 1978, pp 199.

3 J. Fabre, In *Modelling and Experimentation in Two-phase Flow*, ed. V. Bertola, Springer, New York, 2004, pp. 79-116.